JCE

Numerical study of using multi-direction angle wire mesh as a confinement system for confined masonry under horizontal cyclic loads

Muhammad R. Hidayat[a*] , Ahmad B. Habieb[b] , Wahyuniarsih Sutrisno[b]

Correspondence

[a]Master Student in the Civil Engineering Department, Institut Teknologi Sepuluh Nopember, ITS Campus, Sukolilo, Surabaya 60111, Indonesia.
[b]Lecturer of Civil Engineering Department, Institut Teknologi Sepuluh Nopember, ITS Campus, Sukolilo, Surabaya 60111, Indonesia.

Corresponding author email address:
rifathidayat218@gmail.com

Abstract

Indonesia was located in a seismically active region and was situated between three tectonic plates. The construction resilience that met the requirements was necessary in earthquake-prone areas. The purpose was to protect and reduce the risk of severe damage caused by significant seismic loads. However, more than 70% of buildings in developing countries like Indonesia utilized the Confined Masonry (CM) structural system. The implementation of CM systems in Indonesia often led to fatal damages during earthquakes. Due to the severity of these damages, the addition of reinforcement systems to CM became one of the options to address the shortcomings of the CM system. There were various types of materials that could be used as reinforcement, such as steel cages, polymers, polypropylene bands, bamboo meshes, and plastic materials. This study investigated the utilization of ferrocement layers as reinforcement material for CM structural system panels. The specimen panels used had a width of 2300 mm and a height of 1370 mm. The specimens in the research were numerically modeled using the ABAQUS/explicit program. The research variation focused on the influence of the wiremesh sheet orientation angle. The number of variations for the ferrocement layer was one layer with angle configurations of 0, 45, and 60 degrees. This reinforcement layer was applied to one side of the CM panel. As a comparison, results from the control specimen were included. The hysteresis curve, energy dissipation, stiffness degradation, and damage patterns were evaluated in this research.

Keywords

Confined masonry, retrofitting, ferrocement, numerical analysis, simplified-micro model, in-plane loading seismic, direction angle wiremesh

INTRODUCTION

Earthquakes frequently occurred in Indonesia due to its location in an area of three tectonic plates. Being situated in this seismically active zone made Indonesia prone to high seismic activity. The high frequency of earthquakes in Indonesia presented significant challenges in designing and ensuring the quality of buildings to withstand seismic forces. However, the majority of buildings in Indonesia were constructed using the Confined Masonry (CM) structural system. According to Banerjee et al. in 2020, more than 70% of buildings in developing countries adopted the CM structural system, where the load-bearing walls made of red bricks also contributed to the resistance against seismic forces. However, the use of CM systems in Indonesia often failed to meet the requirements for earthquake-resistant buildings [1].

The history of using the Confined Masonry (CM) structural system in Indonesia traced back to the colonial era under Dutch rule. During that time, buildings commonly employed masonry construction, where brickwork was used as the load-bearing material for both external and internal loads. The buildings constructed during the Dutch colonial period typically consisted of one to two layers of brick and utilized brick pillars. This construction system was known as Unreinforced Masonry (URM). The materials used in colonial-era buildings had

specifications that were no longer in use after the end of the colonial period [2]. After Indonesia gained independence, brick remained a commonly used construction material. However, the number of layers and thickness of bricks used was reduced to half a layer due to cost considerations. Using only one or two layers of bricks would have significantly increased construction costs at that time. As a result of the reduced number of brick layers, the seismic behavior of the structures became brittle, leading to sudden collapses. This behavior prompted the use of columns and perimeter beams as regular binding elements in residential buildings, commonly referred to as practical columns and perimeter beams at that time.

The survey conducted by ITB (Institut Teknologi Bandung) regarding the utilization of Unreinforced Masonry (URM), Confined Masonry (CM), and non-engineered systems in residential buildings in rural and urban areas of Yogyakarta, West Java, and West Sumatra provinces yielded the following results: In rural areas:63% of the surveyed buildings adopted the URM system.8% of the surveyed buildings utilized the CM system.29% of the surveyed buildings were categorized as non-engineered structures.In urban areas: 16% of the surveyed buildings were constructed using the URM system. 66% of the surveyed buildings employed the CM system. 18% of the surveyed buildings were classified as non-engineered

structures. These findings indicate that in both rural and urban areas, the adoption of the CM system is more prevalent compared to the URM and non-engineered systems.

Table 1 Survey on the utilization of URM, CM, and Non-engineering systems in rural and urban areas [3]

Area	%Total		
	URM	CM	Non
Rural	63	8	29
Urban	16	66	18

According to data from the National Disaster Management Agency of Indonesia, the damage caused by a mild earthquake in South Halmahera in February 2021 resulted in the destruction of 60 units of simple residential houses. On the other hand, a major earthquake in Central Sulawesi, which affected four cities including Palu, Donggala, Sigi, and Parigi, resulted in 2,256 fatalities and displaced 223,751 people. The estimated losses from the earthquake disaster were around 13.82 trillion Indonesian rupiahs. These statistics serve as evidence for the need to have earthquake-resistant buildings in Indonesia to mitigate the impacts of seismic events.

The commonly used CM system in buildings in Indonesia tends to exhibit brittleness during seismic events and lacks detailing. In the CM system, the binding elements are located around the brick panels. Unlike reinforced concrete systems, where the reinforced concrete elements serve as the primary load-bearing elements, the CM system relies on the composite action between the brick material and the binding elements to resist external forces. The binding elements in the CM system typically consist of reinforced concrete, which often fails to meet the requirements for effectively resisting external forces. The composite action between the brick material and the binding elements requires a mechanism for stress distribution at the interface of these materials to distribute the occurring stresses. As a result, the CM system exhibits complex behavior. This complexity leads to different failure mechanisms and various failure theories in the CM system.

The concept of failure in the CM system was first proposed by Meli in 1973. According to this approach, the walls with binding elements that have sufficient transverse reinforcement can prevent cracking and diagonal failure in the corner regions of the walls. This reinforcement arrangement enhances the ductility of the system when shear failure mechanisms occur [4]. In 1996, Alcocer furthered the research on failure theories in the CM system based on the damage observed in CM specimens. Four types of failure and their corresponding mechanisms were identified in the CM system: compression failure, shear-sliding failure, diagonal-tension failure, and rocking failure. These failure modes provide insights into the different ways in which the CM system can fail under various loading conditions [5]. While there are theoretically four types of failures that can occur in the CM system, the most common failure type during seismic events is diagonal-tension failure. However, the actual failure mechanism depends on the combination of existing conditions in the CM system and qualitative and quantitative factors such as wall geometry, material conditions, magnitude of loads, and the presence of restraints or boundary conditions. According to the theory proposed by Yekrangnia et al. in 2017, when CM specimens are subjected to horizontal in-plane lateral loads, there are three potential failure types in the wall panels: shear-sliding, diagonal-tension, and toe crushing. Additionally, there are three types of damage observed in the binding column elements: shear failure at the bottom of the element opposite to the direction of the applied force, tensile failure at the bottom of the element in the direction of the applied force, and compressive failure at the bottom of the element opposite to the direction of the applied force [6].

Numerous studies have been conducted over the past few decades to enhance the seismic resilience of CM systems. Retrofitting techniques for CM panel walls have been investigated using various materials, including steel cage, polymers, polypropylene bands, bamboo meshes, and plastic materials. These studies aim to improve the structural behavior of CM systems under seismic loading by strengthening or reinforcing the existing components or adding supplementary elements to enhance their resistance to earthquake forces. The selection of retrofitting materials depends on factors such as their mechanical properties, compatibility with the existing CM system, ease of installation, and cost-effectiveness. The research in this area contributes to the development of effective retrofitting strategies to mitigate the vulnerability of CM structures during seismic events [7]. In a study conducted by De Santis et al. in 2015, U-shaped brick wall specimens were subjected to seismic loads on a shaking table. The objective of this research was to investigate the use of retrofitting systems with steel reinforced grout as a material for seismic strengthening. The results of the study showed that the use of reinforcement materials increased the resistance of the specimens by up to 5.1 times compared to the control specimens without retrofitting. Another research study focused on the use of polypropylene (PP) bands as retrofitting materials. The results of this study demonstrated an improvement in energy dissipation capacity, deformation capacity, and shear resistance by 3.3 times, 8.53 times, and 1.62 times, respectively, compared to the non-retrofitted specimens. These studies highlight the effectiveness of retrofitting techniques using different materials in enhancing the seismic performance of CM structures. The use of steel reinforced grout and PP bands as retrofitting materials can significantly increase the structural resilience and resistance of CM systems to seismic forces [8]. A study on retrofitting large-scale wall panels was conducted by Heydariha et al in 2019, using PP bands as the reinforcement material. The results of the study showed a significant improvement, with an increase in specimen ductility up to three times greater and energy dissipation value up to twice as high as the specimens without reinforcement. There are various opinions and perspectives regarding the selection of retrofitting materials for brick walls and CM systems. Several determining factors for choosing reinforcement materials include material strength, cost, the environmental impact of the materials chosen, and the availability of easily accessible materials in the local market [9].

The ferrocement technology, which utilizes wiremesh and mortar matrix as its main materials, is a viable option

for retrofitting techniques in brick specimens and CM systems. Ferrocement materials can create composite forces when the mortar is hydrated and adheres to the wiremesh. B. Kondraivendhan conducted a study in 2009 on the effects of adding reinforcement layers using ferrocement to reinforced concrete, showing a significant improvement in compressive strength and strain values [10].

In a study conducted by Chourasia et al in 2019, a comparative analysis was conducted on different materials used for retrofitting brick wall panels. Six types of materials were investigated, including plastic cement bag mesh (PCBM), nylon mesh (NM), polypropylene band (PBM), industrial geogrid mesh (IGM), ferrocement with welded wiremesh (WWM), and chicken wire mesh (CWM). The testing conducted included evaluating compressive strength, shear strength, and the cost required for retrofitting using each material. In the results of the study, the behavior of each reinforcing material showed a non-linear stress-strain graph. The WWM material demonstrated significant results in compressive strength evaluation with a strength of 6.48 N/mm^2, while the PCBM and IGM materials showed compressive strength performances of 6.09 N/mm^2 and 6.03 N/mm^2, respectively. The other materials exhibited compressive strength performances lower than these three materials. In terms of material cost, the WWM, PCBM, and IGM required costs of 14,879 rupiah/m^2, 25,879 rupiah/m^2, and 75,986 rupiah/m^2, respectively [11]. Therefore, the study demonstrates that the use of ferrocement material with welded wiremesh fiber has advantages in terms of strength, performance, and cost-effectiveness.

The orientation of wiremesh in ferrocement reinforcement has a significant influence on its strength contribution. The proper orientation of wiremesh is crucial in enhancing the structural performance of ferrocement panels used in brick wall construction. This study aimed to investigate the effect of wiremesh orientation on the flexural strength and crack resistance of ferrocement panels. Experimental programs were conducted by fabricating panels with horizontal and vertical wiremesh orientations, followed by flexural load testing. The results of the study showed that panels with horizontal wiremesh orientation exhibited significantly higher flexural strength and better crack resistance compared to panels with vertical orientation. This can be attributed to the improved load distribution and superior crack control mechanism provided by the horizontal wiremesh. These findings provide valuable insights for structural engineers and construction professionals in optimizing the design of ferrocement panels for brick wall applications [12].

The use of numerical analysis in research conducted on masonry structural reinforcement has been widely utilized and applied in recent years [13] [14] [15]. The utilization of numerical analysis in research is considered to be cost-effective and can reduce the time required. The modeling of masonry structural elements in numerical analysis can be carried out using various modeling methods. The categorization of masonry structural modeling can be divided into detailed-micro modeling, simplified-micro modeling, and macro-modeling.

In micro-detailed modeling, simulations are carried out by modeling individual parts and elements in detail.

Brick and mortar elements are modeled using continuum elements, and the interaction between mortar and brick is represented using cohesive interfaces. The use of the detailed-micro method can produce accurate modeling outputs, but it is considered computationally expensive. Therefore, this method is often limited to small-scale modeling.

An alternative to the computationally expensive micro-detailed modeling approach is the simplified-micro modeling method. In simplified-micro modeling, the brick and mortar elements are combined into a single entity called the expanded unit. Instead of explicitly modeling the mortar, the input data for the expanded unit is a combination of the properties of both materials. Cohesive interfaces are used as inputs to capture the behavior between the expanded unit elements. This approach allows for a reduction in computational costs while still considering the interaction between the brick and mortar elements.

The macro-modelling method is a technique used to model masonry systems by employing a homogeneous material approach. In macro-modelling, the masonry elements are modeled using a single homogeneous material, without considering the interface between the masonry units and mortar or the interactions between them. This approach involves the use of material properties that represent the combined behavior of the materials [16]. Indeed, the use of the macro-modelling method is often employed to obtain practical results that aim to capture the generic behavior of the investigated specimens. By employing a simplified and homogenized representation of the masonry system, the macro-modeling approach allows for efficient analysis and provides insight into the overall response of the structure. This can be particularly useful in obtaining general trends, design guidelines, or evaluating the overall structural behavior of masonry systems under different loading conditions. However, it is important to note that the macro-modeling approach may not capture the finer details and localized effects within the masonry system [17].

RESEARCH SIGNIFICANCE

The research aimed to evaluate the use of ferrocement layer reinforcement in CM systems. The influence of various wiremesh orientation angles applied to the panel's side was assessed. The evaluation focused on the generated hysteresis curves, energy dissipation of each specimen, and stiffness degradation with increasing applied loads. The ferrocement layer consisted of a single layer of reinforcement applied to one side of the panel. The wiremesh orientation angles used were 0, 45, and 60 degrees from the horizontal angle of the specimen. The patterns of damage and plasticity that occurred during loading were also observed. The benefits obtained in this study aimed to achieve a comparative analysis of the use of different orientations of wire mesh in ferrocement, with the expectation of providing an efficient alternative for practical applications. Additionally, the results of this research could be further developed in subsequent studies and serve as a reference for future research endeavors.

METHODOLOGY

The specimens will be named accordingly based on the combinations of wiremesh orientation angles and the number of ferrocement layers used. For example, S1-0, S1-45, and S1-60 represent specimens with a single layer of ferrocement and wiremesh orientations of 0, 45, and 60 degrees, respectively. The control specimen, without ferrocement reinforcement, will be named CW-1-1.

Table 2 Research specimen variations for CM system

Model	Wall State	Angle of Wiremesh
CW-1-1	Without Retrofitting	-
S1-0	Single Sided Single Layer Retrofitting	0
S1-45	Single Sided Single Layer Retrofitting	45
S1-60	Single Sided Single Layer Retrofitting	60

and an ultimate strength of 405 MPa. The ratio of longitudinal reinforcement to transverse reinforcement is chosen based on specific criteria to enhance the flexural capacity of the wall panel and accommodate diagonal-tension failure during in-plane cyclic horizontal loading.

In the numerical modeling of this research, the mortar layer is eliminated and replaced with a combination of brick and mortar elements. This combination of brick and mortar elements is called an expanded unit element. The expanded unit element used in this modeling has dimensions of 250x125x63 mm in terms of length x width x height. The number of layers used in the CM specimen panel consists of two layers of expanded unit elements. The arrangement pattern of the expanded unit elements alternates in opposing directions from one unit to another.

The reinforcement layer in each specimen has a thickness of 25 mm for a single layer of ferrocement
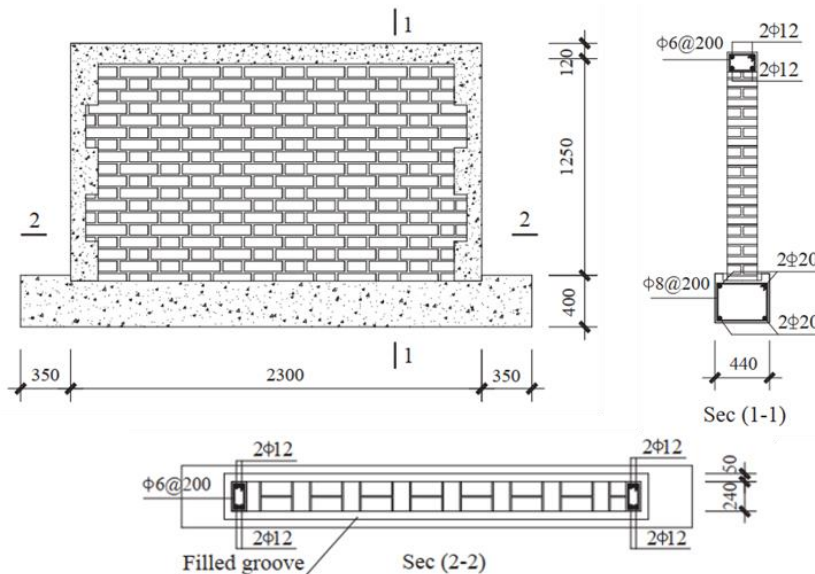
Figure 1 Configuration of CM system specimen

A. SPECIMEN CONFIGURATION

The specimen configurations are based on the assumption of using CM panels commonly found in low-rise to mid-rise buildings. All CM panel specimens are designed with dimensions of 2300 mm in length, 1370 mm in height, and a masonry thickness of 240 mm. These dimensions result in a height-to-length ratio of 0.6. The CM system includes tie elements, consisting of tie beams and tie columns. The tie columns and tie beams have dimensions of 240 x 120 mm in length and width, respectively. The tie columns are positioned on both sides of the masonry panel, while the tie beams are placed on the top side of the panel. At the bottom of the panel, there is a restraining beam measuring 440 x 400 mm. The bottom layer of bricks is embedded into the top surface of the restraining beam with a depth of 35 mm, aiming to prevent sliding damage at the bottom of the wall panel and avoid premature failure of the specimen.

The restraining beam elements are reinforced with 4 longitudinal bars of 12 mm diameter. The longitudinal reinforcement has a yield strength (f_y) of 372 MPa and an ultimate strength (f_u) of 405 MPa. In addition to the longitudinal reinforcement in the restraining beam, both longitudinal and transverse reinforcement are applied in the tie beam elements. The transverse reinforcement consists of 6.5 mm diameter bars with a yield strength of 338 MPa

reinforcement. Each layer of ferrocement reinforcement contains wire mesh with an appropriate orientation angle for the specific specimen. The variations of angles used are 0, 45, and 60 degrees. The wire mesh used has a size of No. 4 with a diameter of 1 mm for each wire fiber. The wire mesh is positioned in the middle of the ferrocement layer, precisely at 12.5 mm for each ferrocement layer. Mortar is used in the ferrocement elements to create composite action between the wire mesh and mortar.

B. MATERIAL MODELS USED IN NUMERICAL ANALYSIS

Concrete Damage Plasticity (CDP) is used in the numerical modeling of concrete elements and extended units. The adoption of the CDP material model allows for the simulation of the nonlinear behavior of concrete, extended units, and mortar materials. The CDP model accurately captures the cracking and ultimate failure of these materials under tension and compression. Typically, the damage evaluation in tension and compression follows an isotropic scalar approach, considering the characteristic features of material damage [18].

The use of Concrete Damage Plasticity (CDP) is employed in the numerical modeling of concrete elements and extended units. The CDP material model is used to

(a) Wiremesh 60 degree orientation

(b) Wiremesh 45 degree orientation

(c) Wiremesh 0 degree orientation
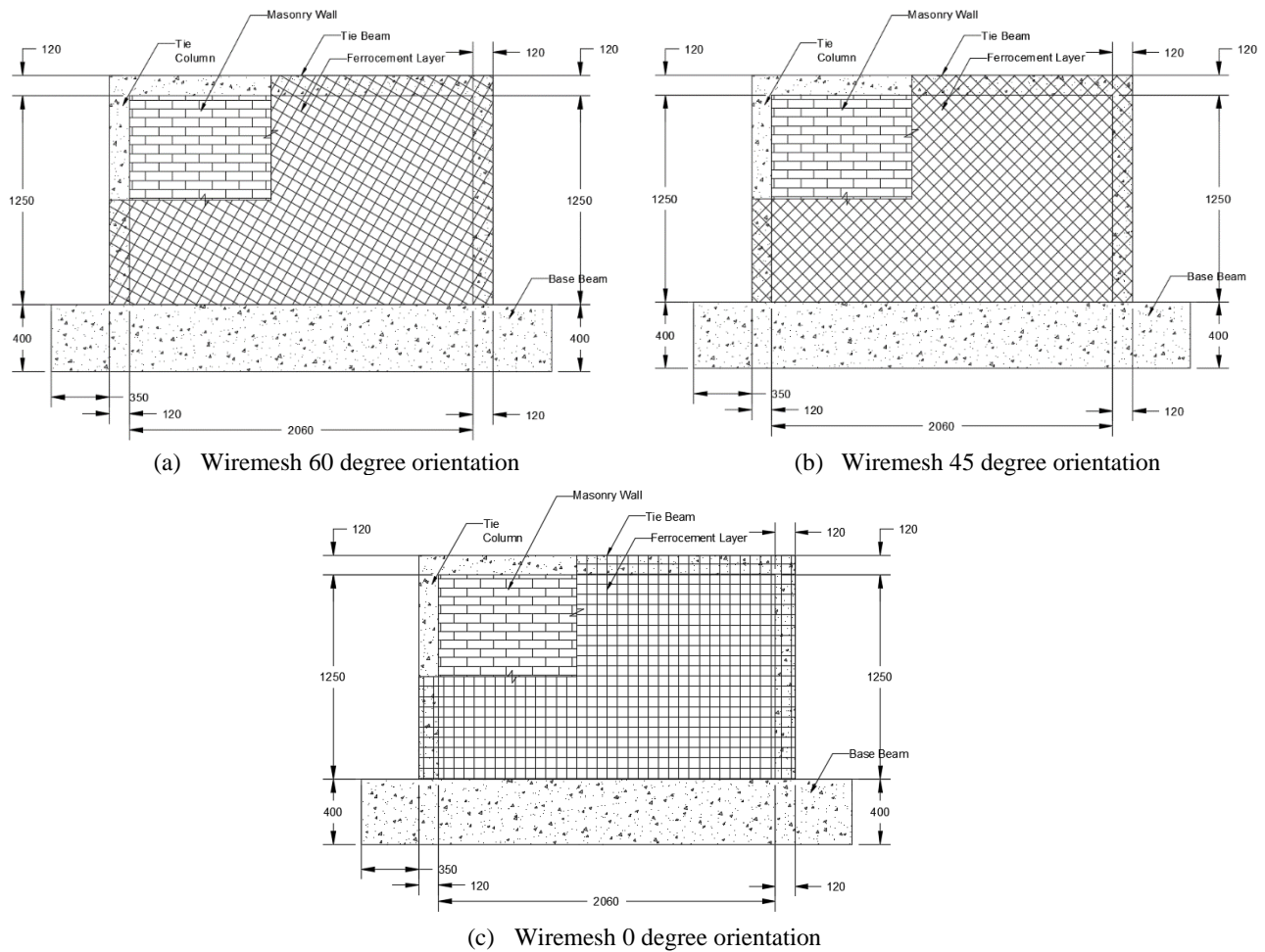
Figure 2 Configuration of wiremesh angle

simulate the nonlinear behavior of concrete, extended units, and mortar. The CDP model simulates cracking during tensile loading and material failure under compressive loading. Generally, these cracking and failure behaviors exhibit characteristics of an isotropic scalar damage evaluation [19].

In the CDP model, the concrete material adopts the stress-strain curve specified by the Chinese Code GB50010-2010, which is applied to both tensile and compressive loading conditions. The stress-strain curve is then converted into a plastic stress-strain curve, and damage parameters are utilized as input data for the material in the numerical program interface. There are five plasticity parameters used to define the CDP material behavior.

The numerical solution method used is dynamic explicit, and thus the viscosity parameter is set to zero. The other four parameters are necessary to complete the definition of the yield surface. The four additional parameters required to complete the definition of the yield surface are determined as follows: The eccentricity parameter (ε), which controls the potential deviation from its asymptote, is set to the default value of 0.1.

- The Kc parameter, which is involved in the yield function and used to define the shape of the failure surface in the deviatoric plane, is set to the default value of 0.667.

- The ratio of fb_0/fc_0, which is one of the parameters used to define the yield function, can be obtained through the proposed input parameter identification approach in the Labibzadeh literature of 2015 [20] [21]. This parameter can greatly influence the results of the numerical study. Therefore, in the research conducted by Van Zijl, four standard tests were performed: uniaxial compression test, uniaxial tensile stress test, four-point bending test, and shear test using the Lasipescu method. From the results of these tests, the appropriate value of fb_0/fc_0 was found to be 1.16 [22].

- The dilatation angle (ψ), which involves non-associated behavior and is measured on the p-q plane under high confining conditions, is set to a value of 30 degrees in the modeling. [20][21].

As an addition, the CDP material model is also applied to the mortar material, which acts as the binder for the ferrocement wiremesh. The mortar material has the following CDP plasticity parameters: ε (eccentricity parameter), K_c (ratio of biaxial compressive strength to uniaxial compressive strength), fb_0/fc_0 ratio (ratio of tensile strength to compressive strength), and ψ (dilatation angle), with respective values of 0.1, 0.667, 1.05, and 36 degrees. The selection of these parameters is based on evaluation and validation. Unlike the use of the GB50010-2010 code to establish the stress-strain curve, the mortar material adopts the regulations of Eurocode 2. The assumed stress-strain curve model is derived from the validation of

numerical and experimental models that comply with Eurocode 2. Eurocode 2 provides equations (equations 1, 2, and 3) to obtain the stress-strain curve.

$$\sigma = \sigma_{cu} \frac{k\eta - \eta^2}{1 - (k-2)\eta} \qquad (1)$$

$$\eta = \varepsilon / \varepsilon_{c1} \qquad (2)$$

$$k = \frac{1,05 \, E_c \, \varepsilon_c 1}{\sigma_c u} \qquad (3)$$

The equation above, where $\sigma_{cu} = f_{cu}$ represents the peak stress, exhibits a stress-strain curve as shown in Figure 3. The CDP material model applied to the expanded unit has the following plasticity parameters: Kc, f_{b0}/f_{c0} ratio, ψ (dilatation angle), with respective values of 0.1, 0.667, 1.05, and 36 degrees. To simulate material damage under compression conditions in the expanded unit, the uniaxial compressive stress-strain equation is used, which is derived from the research conducted by Kaushik et al [23]. To simulate damage under tensile conditions in the expanded unit material, the stress-strain curve follows the bilinear stress-crack softening curve proposed by Kyoungsoo Park in 2008. This curve incorporates a fracture energy concept, where the area under the curve after the peak condition represents the material's fracture energy [24].
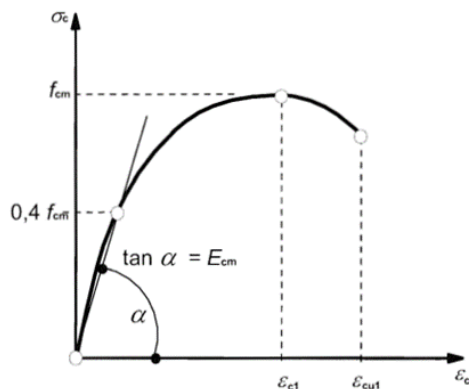
Figure 3 Eurocode 2 stress-strain curve

The constitutive model used for the reinforcement elements follows a bilinear behavior, representing the elastic and yielding conditions. For the 12 mm diameter reinforcement bars, the yield strength and ultimate strength are 372 MPa and 405 MPa, respectively. The maximum strain is 0.2, which, in the context of CDP material, corresponds to an inelastic strain of 0.19814. Similarly, for the 6.5 mm diameter reinforcement bars, the yield strength and ultimate strength are 338 MPa and 405 MPa, respectively, and the maximum strain is 0.18, corresponding to an inelastic strain of 0.17831. The simplified bilinear curve is also applied to the wire mesh material. The wire mesh has a unit weight of 7.48 t/m³. In the elastic behavior, it has an elastic modulus of 210,000 MPa and a Poisson's ratio of 0.3. In the plastic behavior, the input data for the wire mesh includes the yield stress and the plastic strain up to the ultimate strength. The assumed values for the yield stress and ultimate strength are 600 MPa, while the plastic strain ranges from 0 to 0.1.

In the simplified micro model used in masonry panels, the interaction between expanded units is simulated using

a cohesive surface-based model to capture the bonding and behavior between expanded units. The cohesive behavior is differentiated into bed joints (horizontal bonding) and head joints (vertical bonding). The surface-based cohesive behavior is further divided into elastic and plastic conditions. The elastic interaction behavior refers to the equation formulated by Lourenco in 1996. The elastic behavior is formulated based on linear traction-separation behavior, which is related to the damage in the expanded unit material. In general, the linear behavior of expanded units is expressed in the form of an elastic stiffness matrix [25].

$$K_{nn} = \frac{E_u E_m}{h_m (E_u - E_m)} \qquad (4)$$

$$K_{ss} \text{ and } K_{tt} = \frac{G_u G_m}{h_m (G_u - G_m)} \qquad (5)$$

In the plastic condition, the expanded unit material exhibits linear response followed by the occurrence of cracking. Cracking occurs when the damage initiation criterion is reached, which is defined by the traction conditions between expanded unit elements. A quadratic stress criterion equation is used to define the initiation of damage. This equation is employed because it effectively predicts the initiation of cracking in the interaction between expanded units [26]. The equation is expressed as Eq. 4.

$$\left(\frac{t_n}{t_n^{max}}\right)^2 + \left(\frac{t_s}{t_s^{max}}\right)^2 + \left(\frac{t_t}{t_t^{max}}\right)^2 = 1 \qquad (6)$$

The exclusion of compressive stresses in the normal direction affects the fracture behavior of joints, as indicated by the Macaulay bracket in Equation (4). The cracking of masonry joints under tension is controlled by the specified tensile strength of masonry joints. The description of the critical shear stress of joints before failure is given by the Mohr-Coulomb failure Equation (5).

$$\tau_{crit} = c + \mu\sigma_n \qquad (7)$$

The calculation of shear strength in masonry joints is derived from Equation (5), which takes into account the cohesion, coefficient of friction, and normal compressive stress. In this regard, scrit is utilized to define the shear strength of masonry joints (t_s^{max} and t_t^{max}). Similarly, the potential improvement in shear behavior prior to failure caused by frictional resistance is incorporated into the crack initiation criterion of masonry joints within the surface-based cohesive model.

Furthermore, the coefficient of friction in masonry joints is defined to simulate the shear sliding behavior after failure (tangential behavior). The critical sliding shear stress ($\tau_{sliding}$) is determined by the friction law Equation (6), which follows a linear relationship between the coefficient of friction and normal compressive stress.

$$\tau_{sliding} = \mu\sigma_n \qquad (8)$$

The aforementioned friction formulation implies that the masonry units will experience sliding when the shear stress in the failed masonry joints exceeds the critical sliding shear stress ($\tau_{sliding}$).

Upon reaching the damage initiation criterion, the propagation of cracks in the masonry joints results in a gradual degradation of stiffness at a specified rate,

ultimately leading to the complete loss of strength and joint failure. Consequently, Equation Lourenco 1996 is modified and presented as Equation (7):

$$t = (1 - D) K \delta \qquad (9)$$

The variable D represents the evolution of damage, where its value increases from 0 to 1 in accordance with the continuity of traction stresses once the damage initiation criterion is met. In this study, a linear damage evolution variable is assumed, and it is defined by specifying the energy dissipated during the damage process (see Figure 4).
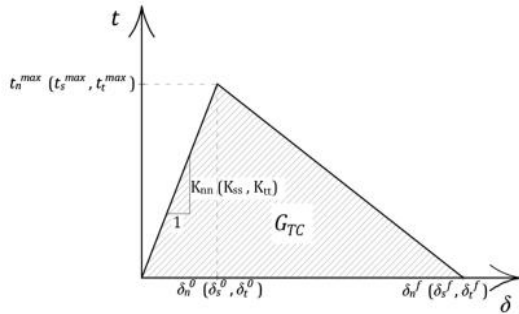
Figure 4 Linear damage evolution of cohesive element

The damage variable can be expressed as follows:

$$D = \frac{\delta_{eff}^{f} \left(\delta_{eff}^{max} - \delta_{eff}^{0} \right)}{\delta_{eff}^{max} \left(\delta_{eff}^{f} - \delta_{eff}^{0} \right)} \qquad (10)$$

The effective separation δ_{eff} mengacu pada persamaan pada [27].

$$\delta_{eff} = \sqrt{\left(\delta_n \right)^2 + \delta_s^2 + \delta_t^2} \qquad (11)$$

The effective separation at complete failure δ_{eff}^{f}, is also expressed as:

$$\delta_{eff}^{f} = \frac{2 G_{TC}}{t_{eff}^{0}} \qquad (12)$$

The effective separation at the point of complete failure of the joint is represented by δ_{eff}^{f}, while δ_{eff}^{0} denotes the relative effective separation when damage initiates in the joints. Additionally, δ_{eff}^{max} corresponds to the maximum effective separation achieved during the loading history. The critical mixed-mode fracture energy, denoted as G_{TC}, is determined using the Benzeggagh-Kenane (BK) law [20]. This law is considered the most suitable when the critical fracture energies for both shear directions (mode II and mode III) are equal, which is the case in masonry joints. The exponent, η, in the BK law is set as 2, assuming brittle behavior in masonry joints [28] . The critical fracture energy, G_C, for the mixed-mode in the BK law can be expressed as follows:

$$G_{TC} = G_{IC} + (G_{IIC} - G_{IC})(\frac{G_{II} + G_{III}}{G_I + G_{II} + G_{III}})^{\eta} \qquad (13)$$

A summary of the mechanical parameters of mortar, concrete and expanded unit materials under cyclic inplane loading conditions is shown in table 3 and the interaction properties between expanded units are shown in table 4.

Table 3 Mechanical paramater of concrete, mortar ferrocement and brick (expanded unit)

Material	Elastic			Non-Linear			
	E	υ	f_c	f_{cr}	f_{tu}	ε_{to}	G_f
	(MPa)			(MPa)	(MPa)	(%)	(N/mm)
Concrete	29400	0.2	22.33	-	2.23	-	-
Mortar	29725	0.2	39.99	-	2.78	-	-
Brick	7854	0.15	3.18	-	0.6	-	0.15

Table 4. Summary of the interface paramater

	Symbol	Bed Joint	Head Joint
Tension	K_{nn} (MPa)	33.11	28.72
	t_n^{max} (MPa)	0.12	0.09
	G_{sl} (N/mm)	0.022	0.04
Shear	K_{ss} (MPa)	14.4	12.48
	K_{tt} (MPa)	14.4	12.48
	C (MPa)	0.17	0.06
	μ	0.75	0.75
	G_{ssl} (N/mm)	0.22	0.18

To ensure an equivalent elastic response between the expanded masonry units and the original masonry assemblage (consisting of units and mortar), it is necessary to adjust the elastic modulus of the expanded masonry units. This adjustment takes into consideration the moduli of elasticity of the original masonry units and mortar, as well as the geometry of the masonry assemblage. For this purpose, Equation (13) is proposed, assuming a stack bond between the masonry units and a uniform stress distribution in the masonry constituents. The equation is presented as follows:

$$E_{adj} = \frac{H E_u E_m}{n h_u E_m + (n - 1) h_m E_u} \qquad (13)$$

Where E_{adj} is the elastic modulus of the expanded unit, H, hu, and hm represent the height, thickness of the brick, and thickness of the mortar joint, respectively. E_b represents the elastic modulus and shear modulus of the brick material [29] [16] [30].

C. LOADING PROTOCOL

The loading procedure is performed in two stages: force-controlled and displacement-controlled. The force-controlled stage is used until the occurrence of cracks in the specimen. Force-controlled loading is applied gradually with a load increment of 40 kN. In this force-controlled loading scheme, each load increment corresponds to one cycle of loading.

It is then followed by the displacement-controlled loading method. Unlike the force control method, the displacement control method involves loading the specimen in each load increment using two loading cycles. The load increment used is 0.15% drift of the specimen. With a specimen height of 1770 mm, a 0.15% drift corresponds to 2.655 mm. The loading scheme for the confined masonry validation specimen is illustrated in the graph shown in Figure 5.
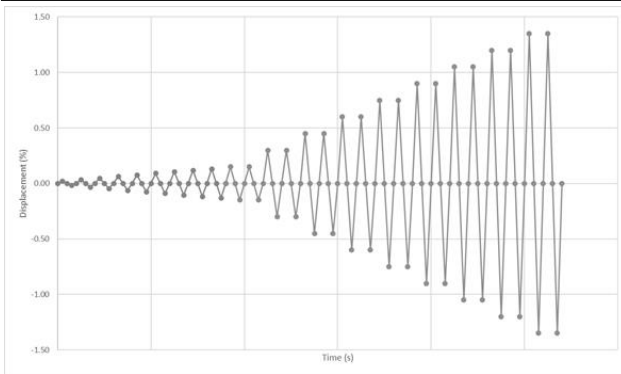
Figure 5 Loading protocol of horizontal cyclic load

D. BOUNDARY CONDITION AND MESH

There are several types of meshing used to simulate the experimental results of the CM system in this numerical study. First, first-order meshing is used with the reduced integration hexahedral continuum (C3D8R) type, with the addition of hourglass control for the expanded unit and concrete materials, which serve as binding elements around the brick wall panels. In addition to these two materials, this type of meshing is also applied to the mortar ferrocement elements and the connector elements used to connect the upper sides of the binding beams. Second, the Linear 2 Node 3D Truss (T3D2) type is used for the reinforcement particle elements, both longitudinally and transversely, in both vertical and horizontal directions. The interaction between the binding elements and the wall panels is modeled using Tie Constraints. This study also applies Tie Constraints to the interaction between the ferrocement reinforcement layer and the surface layer of the wall panels. The use of Tie Constraints is also applied to the double-layered ferrocement specimens in this research variation.

The binding element reinforcement, longitudinal reinforcement, and transverse reinforcement are reinforced using embedded region interaction in the concrete element material. This embedded interaction ensures full compatibility between the reinforcement particles and the concrete material.

The mesh sizes used are 30 mm for the expanded unit material, 50 mm for the longitudinal reinforcement of the binding element, and 25 mm for the transverse reinforcement of the binding element. However, for the concrete frame elements or binding elements, the mesh size varies. A larger mesh size is used at the bottom of the model, gradually decreasing as it approaches the top of the specimen. Additionally, a larger mesh size is used for the out-of-plane direction of the specimen. This approach is an optimization effort to accelerate the model analysis process. Therefore, a mesh size of 100 mm is used at the bottom of the specimen, which then decreases to 50 mm as it approaches the top. For the out-of-plane direction, a mesh size of 100 mm is used.

The dead load, which is generated by the mass of each material, is applied in the initial condition. This is done to account for the self-weight effect on the loading results. In the ABAQUS program, the self-weight is input based on the material density, and then the loading is performed by applying a gravity acceleration of 9.81 m/s^2.

RESULTS AND DISCUSSIONS

A. SPECIMENT CONTROL

Several common characteristics can be observed from the cracking process of the unretrofitted CM walls treated as control specimens. Initially, the walls exhibited a nearly linear behavior until fine stepped shear cracks formed either in the central part or at the top corner. Subsequently, the lateral load continued to increase until reaching the peak load, accompanied by the propagation of existing cracks. With increasing displacement, additional cracks appeared, resulting in the formation of a network of shear cracks. Additionally, two distinct primary diagonal shear cracks formed completely, primarily traversing through the bed and head joints. The analysis results of the hysteresis curve for the CW 1-1 control specimen show an average resistance force of 167.7 kN. After reaching the maximum
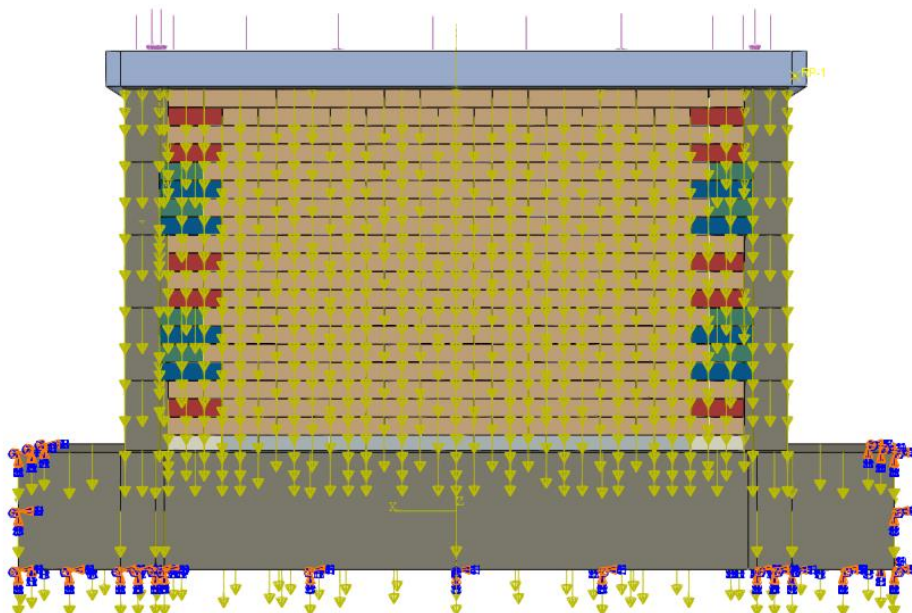
Figure 6 Boundary condition of specimen numerical analysis

force, the resistance of the control specimen gradually decreases. At the end of the testing cycle, the main cracks widen, and damage occurs at the upper corner of the unreinforced CM wall. The gradual decrease in the hysteresis curve indicates that the use of binding elements can enhance the specimen's resistance to horizontal cyclic forces and improve its ductility capacity compared to specimens without binding elements.
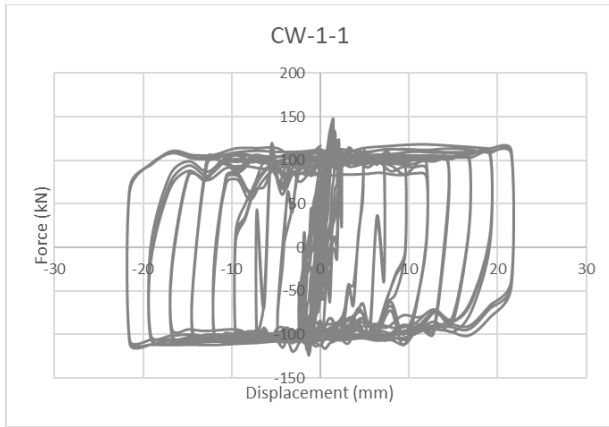
Figure 7 Hysteresis curve of CW-1-1 specimen

B. RETROFITTED WALL

The specimens with one side and one layer of ferrocement reinforcement consist of specimens with the codes S1-0,

S1-45, and S1-60. Each specimen has a variation in the orientation angle, specifically 0, 45, and 60 degrees. The numerical results of the retrofitted specimens exhibit similar characteristics among each other. The stress distribution in these specimens under horizontal loading tends to concentrate in the area of the reinforcement layer and decreases on the opposite side. In the specimen with a 0-degree single-layer orientation, the maximum stress at a displacement of 2.32 mm or at the end of the force-controlled cycle is 17.05 MPa, located in the bottom corner area of the reinforcement layer. The maximum stress gradually decreases in the adjacent region to a stress value of 9.744 MPa.In the specimen with a 45-degree orientation, at the same displacement of 2.32 mm, the maximum stress is also concentrated in the bottom corner area near the direction of the horizontal load, with a maximum stress value of 20.2 MPa. The stress on the other side of the specimen at the maximum stress region decreases to 11.59 Mpa.For the specimen with a 60-degree orientation, the maximum stress at a displacement of 2.32 mm is 18.43 MPa.

The damage patterns and plastic strains in the single-sided layer specimens differ between the reinforced and non-reinforced sides. The observed crack and damage patterns during loading are different on these two sides. On the reinforced side, initial damage occurs at the bottom locations of both ends of the panel. This is observed due to the pressure applied during cyclic loading, and as the
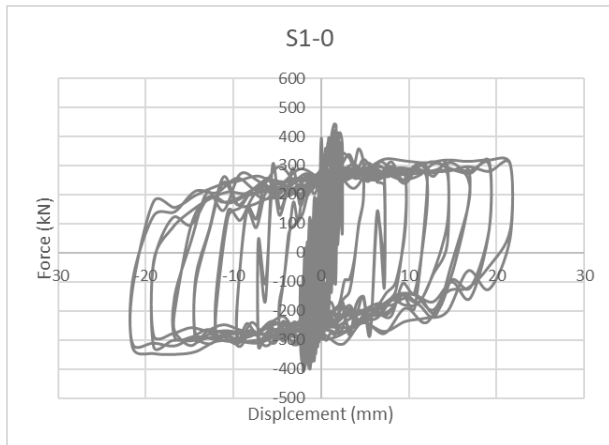
(a)
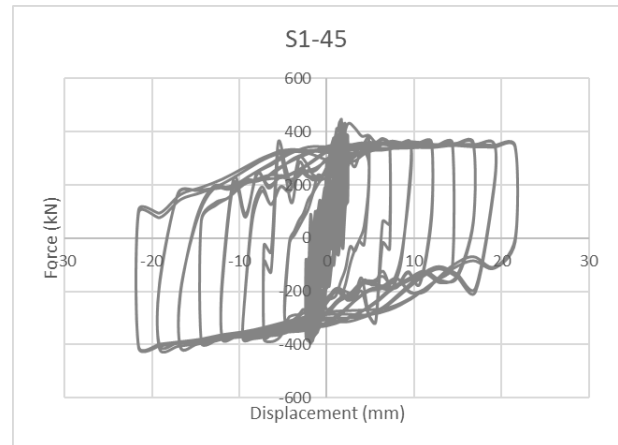
(b)
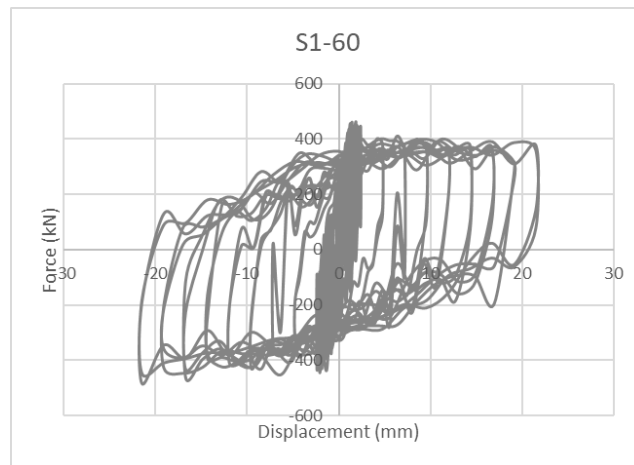
(c)

Figure 8 Plastic strain in CW-1-1, (a) S1-0, (b) S1-45, and (c) S1-60 Specimens.
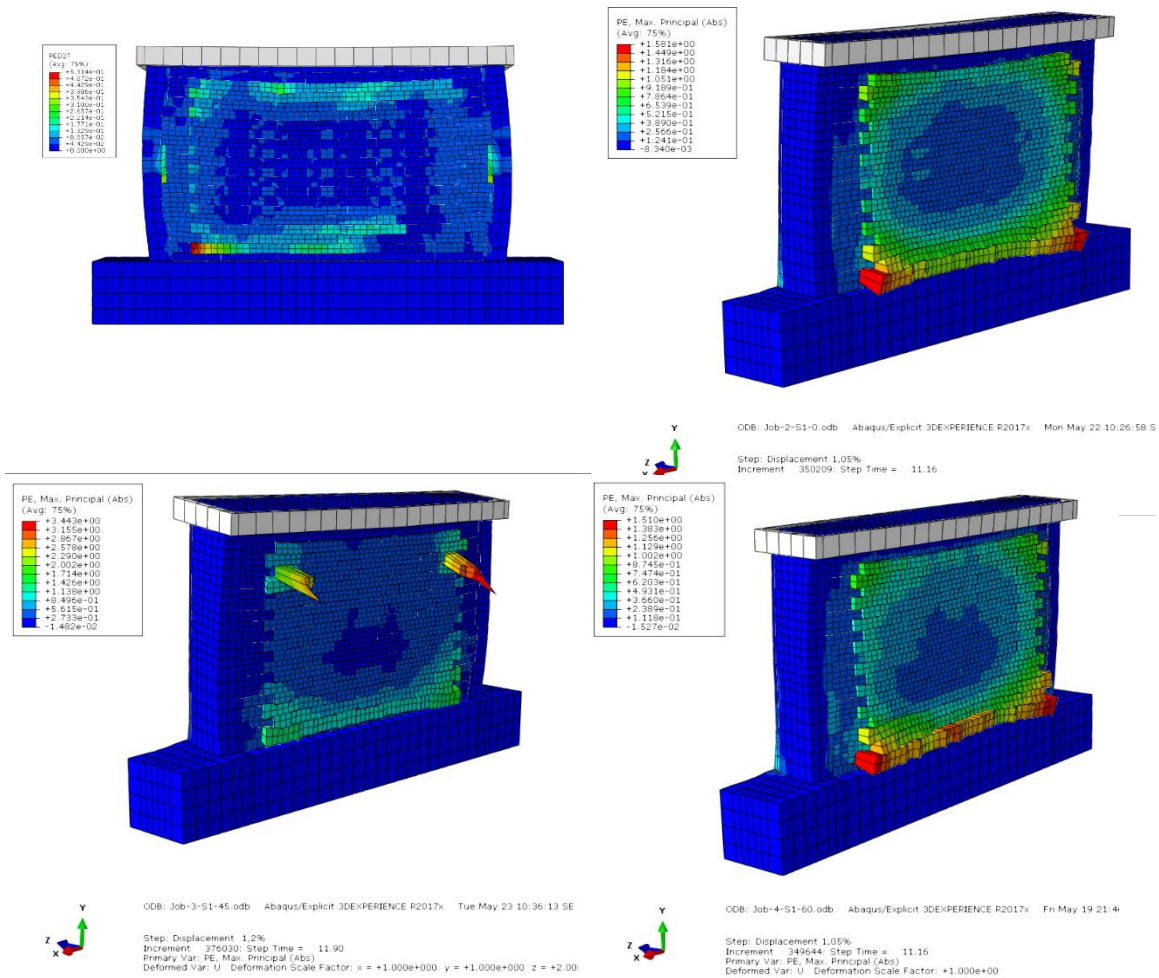
Figure 9 Plastic strain in CW-1-1, S1-0, S1-45, and S1-60 Specimens

Table 5 Disipated energy of all specimen

Specimen	Dissipated Energy			Ratio to Control		
	Force Controlled	Drift 0.6%	Drift 1.35%	Force Controlled	Drift 0.6%	Drift 1.35%
CW-1-1	852.80	3949.40	9385.80	1.00	1.00	1.00
S1-0	2759.40	10283.00	22735.00	3.24	2.60	2.42
S1-45	3046.66	13211.00	25945.00	3.57	3.35	2.76
S1-60	3944.47	11935.00	25724.00	3.45	3.02	2.74

loading increases, the damage extends upwards, forming a U-shaped pattern.

On the non-reinforced side, elastic behavior is observed until cracks appear, also located at the bottom of the panel on both sides. Unlike the reinforced side, the damage spreads more rapidly on this side. The damage starts at the bottom of both ends of the panel and continues with damage to the side/column connectors, followed by dominant damage on the upper side of the panel. Dominant damage is observed on the top and bottom sides of the panel, eventually resulting in collapse of the lower part of the brick wall. In addition to the collapse at the bottom of the panel, torsion due to the difference in stiffness between the reinforced and non-reinforced sides is evident. At the beginning of loading, this torsion event is indicated by uneven stress distribution in the out-of-plane direction of the panel. By the end of the loading cycle, the reinforced side bends towards the non-reinforced side, causing the non-reinforced brick layer to be pushed outward and the ferrocement layer to lift.

The hysteresis curve analysis performed on the single-sided layer retrofitted wall specimens, namely S1-0, S1-45, and S1-60, resulted in maximum resistance forces of 442.68 kN, 447.07 kN, and 445.68 kN, respectively. At these maximum forces, the deflection for each specimen was measured as 1.48 mm, 1.67 mm, and 1.67 mm for S1-0, S1-45, and S1-60, respectively. This indicates a significant increase in each specimen compared to the control specimen. The increase in maximum force values for the specimens is approximately 2.31, 3.02, and 3.02 times larger, respectively.

The concept of energy dissipation in the specimens refers to the absorption and redirection of energy to the effects of damage and deformation in the material. The energy dissipation values in the specimens were measured at the end of the force-controlled loading cycle, at the 0.6% drift of displacement-controlled loading, and at the end of the displacement-controlled loading cycle, 1,35%. Where loading drift 0.6% is chosen because it is a load in the middle of the cycle and for loading 1.35% is chosen to know the result of the end of the loading cycle The overall

energy dissipation values for the specimens are presented in Table 5.

Regarding the stiffness degradation of the specimens, it is illustrated in Figure 10. The observed stiffness degradation in the specimens shows similar patterns in the retrofitted specimens. This confirms that the indication of torsion in the specimens significantly affects the modeling results and the behavior of the specimens under loading conditions.
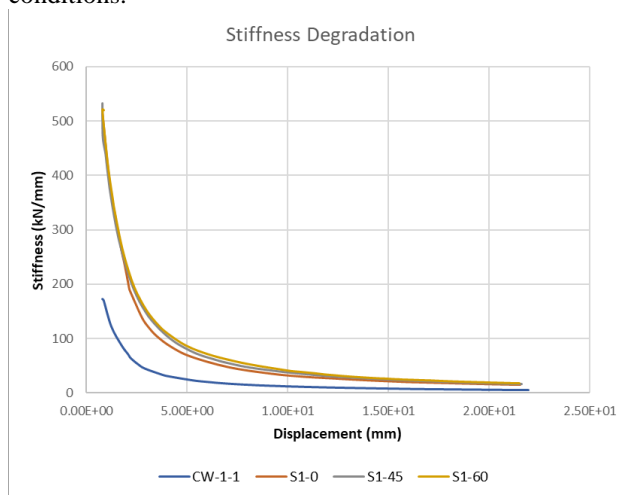
Figure 10 Stiffness degradation of specimen

CONCLUSIONS

The use of reinforcement in CM system specimens has been proven to provide better results and performance compared to URM systems. The improvement in performance is attributed to the increased resistance force of the CM panel and the enhanced ductile behavior of the reinforced CM system.

The behavior of stress distribution in the single-sided reinforced specimens results in stress concentration predominantly on the reinforced side of the panel during loading. The damage behavior of the panel initiates with cracks appearing at the bottom of the panel and then propagating to the sides and top. However, in specimens reinforced with ferrocement, there is an indication of torsional damage, which affects the optimal resistance capacity.

Overall, the reinforcement of CM specimens contributes to increased resistance forces and improved ductility, leading to enhanced performance compared to URM systems. However, it is important to address the torsional damage aspect in reinforced CM systems to optimize their resistance capacity.

REFERENCES

[1] S. Banerjee, S. Nayak and S. Das, "Enhancing shear capacity of masonry wallet using PP-band and steel wire mesh," in IOP Conference Series: Materials Science and Engineering, vol. 431, no. 7, 2018

[2] T. Boen, "Earthquake resistant design of non-engineered buildings in Indonesia," EQTAP Conference, pp. 1–34, 2001.

[3] S. A. A. Gumilang and M. Rusli, "Seismic performance of earthquake resistant simple residential confined masonry house structure based on permen PUPR No.5 of 2016 specification," IOP Conference Series: Earth and Environmental Science, vol. 708, no. 1, 2021.

[4] R. Meli, "Behaviour of masonry walls under lateral loads," Proceedings of the 5th World Conference on Earthquake Engineering, p. 101a, 1973.

[5] S. M. Alcocer, "Comportamiento sísmico de estructuras de mampostería.," Sociedad Mexicana de Ingeniería Estructural, *A.C*, p. 28, 1996, https://reconstruir.org.mx/wp-content/uploads/2017/11/4_comportamiento_sismico_de_estructuras_de_mamposteria_una_revision.pdf (Accessed: April 21, 2023)

[6] M. Yekrangnia, A. Bakhshi and A. Ghannad, "Force-displacement model for solid confined masonry walls with shear-dominated failure mode," Pacific Conference Earthquake Engineering, no. 56, pp. 1–6, 2017.

[7] K. Meguro, "Technological and social approaches to achieve earthquake safer non-engineered houses," 14th World Conference on Earthquake Engineering (14WCEE), 2008.

[8] J. W. D. Santis, "Seismic performance of masonry walls retrofitted with steel reinforced grout," Pacific Conference Earthquake Engineering, no. 056, pp. 1–6, 2015,.

[9] M. Bruneau, "Seismic evaluation of unreinforced masonry buildings — a state-of-the-art report," Canadian Journal of Civil Engineering, vol. 21, no. 3, pp. 512–539, 1994.

[10] B. Kondraivendhan and B. Pradhan, "Effect of ferrocement confinement on behavior of concrete," Construction and Building Materials, vol. 23, no. 3, pp. 1218–1222, 2009.

[11] A. Chourasia, S. Singhal and J. Parashar, "Experimental investigation of seismic strengthening technique for confined masonry buildings," Journal of Building Engineering, vol. 25, no. June, p. 100834, 2019.

[12] O. Lalaj, Y. Yardım and S. Yılmaz, "Recent perspectives for ferrocement," Research on Engineering Structures and Materials, vol. 1, no. 1, 2015.

[13] H. Shakib, S. Dardaei, M. Mousavi and M. K. Rezaei, "Experimental and analytical evaluation of confined masonry walls retrofitted with CFRP strips and mesh-reinforced PF shotcrete," Journal of Performance of Constructed Facilities, vol. 30, no. 6, pp. 1–11, 2016.

[14] M. F. Akbari, D. Iranata and D. Irawan, "Finite element modeling of cold-formed steel bolted moment connection," Journal of Civil Engineering, vol. 37, no. 2, p. 60, 2022.

[15] A. Najib, B. Piscesa and H. Alrasyid, "Numerical simulation of reinforced concrete shear wall using 3D-NLFEA," Journal of Civil Engineering, vol. 37, no. 2, p. 55, 2022.

[16] K. F. Abdulla, L. S. Cunningham and M. Gillie, "Simulating masonry wall behaviour using a simplified micro-model approach," Engineering Structures, vol. 151, pp. 349–365, 2017.

[17] B. Borah, H. B. Kaushik and V. Singhal, "Finite element modelling of confined masonry wall under in-plane cyclic load," IOP Conference Series: Materials Science and Engineering, vol. 936, no. 1, 2020.

[18] U. M. D. E. C. D. E. Los, Non linear mechanic of reinforced concrete. (New York and London: Spon Press Taylor and Frac), 2003.

[19] A. B. Habieb, M. Valente and G. Milani, "Finite element analyses on a small masonry house prototype retrofitted using frp strips," Journal of Civil Engineering, vol. 35, no. 2, pp. 25–33, 2020.

[20] M. Labibzadeh, "Damaged-plasticity concrete model identification for prediction the effects of CFRPs on strengthening the weakened RC two-way slabs with central, lateral and corner openings," International Journal of Structural Engineering, vol. 6, no. 3, pp. 240–268, 2015.

[21] M. Labibzadeh, M. Zakeri and A. Adel Shoaib, "A new method for CDP input parameter identification of the ABAQUS software guaranteeing uniqueness and precision," International Journal of Structural Integrity, vol. 8, no. 2, pp. 264–284, Jan. 2017.

[22] G. P. A. G. van Zijl, "Improved mechanical performance: Shear behaviour of strain-hardening cement-based composites (SHCC)," Cement and Concrete Research, vol. 37, no. 8, pp. 1241–1247, 2007.

[23] H. B. Kaushik, D. C. Rai and S. K. Jain, "Stress-Strain Characteristics of Clay Brick Masonry under Uniaxial Compression," Journal of Materials in Civil Engineering, vol. 19, no. 9, pp. 728–739, 2007.

[24] K. Park, G. H. Paulino and J. R. Roesler, "Determination of the kink point in the bilinear softening model for concrete," Engineering Fracture Mechanics, vol. 75, no. 13, pp. 3806–3818, 2008.

[25] P. B. Lourenco, J. G. Rots and J. Blaauwendraad, "Two approaches for the analysis of masonry structures: Micro and macro-modeling," *HERON*, vol. 40, no. 4, pp. 313–340, 1995,

[26] R. D. S. G. Campilho, M. F. S. F. de Moura and J. J. M. S. Domingues, "Using a cohesive damage model to predict the tensile behaviour of CFRP single-strap repairs," International Journal of Solids and Structures, vol. 45, no. 5, pp. 1497–1512, 2008.

[27] P. P. Camanho and C. G. Davila, "Mixed-mode decohesion finite elements for the simulation of delamination in composite materials," NASA Technical Reports Server, vol. 211737, no. June, p. 42, 2002,

[28] H. P. Klotz, G. Outzekovsky and H. Elmaleh, "Etude de la fonction parathyrouidienne dans un cas de scl'erodermie. effets th'erapeutiques de la parathormone.," Annales d'Endocrinologie, vol. 24, pp. 859–865, 1963.

[29] M. Deng and S. Yang, "Experimental and numerical evaluation of confined masonry walls retrofitted with engineered cementitious composites," Engineering Structures, vol. 207, January, p. 110249, 2020.

[30] A. Rahgozar and A. Hosseini, "Experimental and numerical assessment of in-plane monotonic response of ancient mortar brick masonry," Construction and Building Materials, vol. 155, pp. 892–909, 2017.